JOURNAL OF GEOPHYSICAL RESEARCH, VOL. 103, NO. D15, PAGES 19,327–19,336, AUGUST 20, 1998

Satellite investigations of fire, smoke, and carbon monoxide during April 1994 MAPS mission: Case studies over tropical Asia

Sundar A. Christopher, Joyce Chou, and Ronald M. Welch

Department of Atmospheric Sciences, University of Alabama in Huntsville

Donna V. Kliche

Institute of Atmospheric Sciences, South Dakota School of Mines and Technology, Rapid City

Vickie S. Connors

NASA Langley Research Center, Atmospheric Sciences, Hampton, Virginia

Abstract. During April 9-19, 1994, the Measurement of Air Pollution from Satellites (MAPS) measured free tropospheric carbon monoxide (CO) concentrations on a near-global basis. For these eleven days the global 1km advanced very high resolution radiometer (AVHRR) Pathfinder data are used to detect fires and smoke over the Indo-Burma region (85°E-110°E; 10°N-30°N). The fire activities are categorized for four major ecosystems that include (1) cropland/natural vegetation mosaic (CNVM), (2) evergreen broadleaf forest (EBF), (3) mixed forest (MFD), and (4) grassland (GL). Using published emission rates between particulate matter and carbon monoxide concentrations from temperate areas, the fire counts along with other information are used to obtain estimates of CO concentrations from the AVHRR data. More than 7000 fires are detected during the study period with 23%, 43%, 24%, and 10% fires in the CNVM, EBF, MFD, and GL ecosystems, respectively. The enhanced CO concentrations over the area of study are either over or downwind of the fires detected by the AVHRR. The preliminary AVHRR estimates of CO concentrations are smaller than the MAPS-measured values by a factor of 4 to 5 for fire counts greater than 200. The differences are attributed to the lack of transport mechanisms and other assumptions in the current model. However, these results show a good potential for using the AVHRR measurements to detect fires and smoke and also to estimate CO concentrations.

1. Introduction

Biomass burning is considered to be a major source of trace gas species and aerosol particles [*Crutzen et al.*, 1979; *Logan et al.*, 1981] which play a pivotal role in tropospheric chemistry and climate [*Crutzen and Andreae*, 1990]. Widely prevalent in the tropics, anthropogenic biomass burning expanded drastically in the last 15 years, due to increased deforestation practices in Brazil's Amazon Basin as well as to clear land for shifting cultivation in South America, southeastern Asia, and Africa [*Seiler and Crutzen*, 1980]. Biomass burning produces large amounts of carbon dioxide, carbon monoxide, water, hydrocarbons, nitrogen oxides, and smoke particles [*Crutzen et al.*, 1979]. Recent estimates have shown that about 114 Tg of smoke is produced yearly in the tropics through biomass burning [*Penner et al.*, 1992], and it could have a significant impact on tropospheric chemistry and global climate.

Although the importance of CO on tropospheric chemistry has been well established, only a few studies have addressed the estimation of CO concentrations on a frequent basis. The Measurement of Air Pollution from Satellites (MAPS) [*Reichle et al.*, 1986; V.S. Connors, unpublished manuscript, 1998] provides the only direct measurements of CO concentrations from space. Other studies [e.g., *Kaufman et al.*, 1990] have used satellite advanced very high resolution radiometer (AVHRR) measurements to obtain indirect information about the emission products from biomass burning. Using satellite data, there are two basic methods to obtain information about the emission products. In the first method *Kaufman et al.*, 1990 measured ratios of particle concentrations and trace gases [*Ward*, 1986] are used to obtain trace gas emissions for different fire conditions. In the second method an estimate of the area burned is first obtained from satellite imagery. Then, the emission of trace gases are obtained by using atmospheric chemistry models [*Seiler and Crutzen*, 1980]. Both of these methods are reviewed in detail by *Kennedy* [1992], and further details can be found in the work of *Kaufman et al.* [1990].

Most of the large biomass burning events occur during the dry season: in South America the dry season lasts from July to October [*Setzer and Pereira*, 1991], and in Africa, January is the peak season for savannah burning north of the equator, and May through June, burning activity is widespread in Zambia, Zaire, Zimbabwe, and Angola. The fires in China and southeastern Asia during April to May are correlated with agricultural practices and uncontrolled burning of remote forests [*Cahoon et al.*, 1992]. In 1994, measurements of CO mixing ratios were made using the MAPS instrument, which flew on the space shuttle during the April 9-19 (SRL-1) mission and the September 30 to October 11

Paper number 97JD01813.
0148-0227/98/97JD-01813$09.00

(SRL-2) mission. During the April mission, several fires were observed in southeastern Asia. In October 1994 a much larger number of fires were observed over southeastern Asia, Indonesia (New Guinea and Borneo), and over much of Australia. Scattered fires were also observed in central South America and Africa. Satellite images and space shuttle photographs from the October mission show giant smoke and haze clouds produced by these fires, which extended over thousands of kilometers. Over these regions, MAPS also detected enhanced CO mixing ratios over and downstream of the burning areas. The CO mixing ratios are higher in October than in April because of the seasonality associated with the burning of grasslands and agricultural debris (e.g., sugar cane fields) in the southern tropics. However, the measured October 1994 CO mixing ratios are nearly 4 times larger than those recorded in April 1994, thus implying the significance of the vegetation-type, distribution, intensity, and extent of biomass burning events, as a factor responsible for such enhancement [*Connors et al. this issue*].

The major focus of the present study is: (1) to detect the fires and smoke from biomass burning for four major ecosystems over the study area and to compare these fire activities with the MAPS-measured CO concentrations, and (2) to use published emission rates between particulate matter and CO concentrations in order to provide preliminary estimates of CO values from AVHRR data. Although urban sources could contribute to the tropospheric carbon monoxide, the current study only examines the relationship between fire activities and MAPS-measured midtropospheric carbon monoxide concentrations.

The paper is organized as follows: Section 2 describes the data set used in this investigation. Section 3 describes the methodology. Section 4 outlines the results, and section 5 concludes the paper.

2. Data

The AVHRR data from the NOAA series of satellites has been used extensively to study land, sea, and atmospheric processes. The AVHRR sensors are placed in a polar-orbiting, Sun-synchronous orbit and have five spectral channels (0.58-0.68 μm, 0.72-1.10 μm, 3.55-3.93 μm, 10.3-11.3 μm, 11.5-12.5 μm). The spatial resolution is 1.1 km at nadir, which is adequate for fire and smoke detection [e.g. *Justice et al.*, 1996; *Kaufman and Nakajima*, 1993; *Christopher et al.*, 1996].

The MAPS instrument, installed onboard the space shuttle, is a nadir-viewing, gas filter correlation radiometer that is designed to measure the global distribution of middle tropospheric carbon monoxide mixing ratios [*Reichle et al.*, 1986, 1990]. This passive remote sensor maintains high effective spectral resolution in the 4.67 μm fundamental band of CO. The instantaneous field of view (FOV) is 20 km^2 at the surface of the Earth, and the data are sampled once each second. The combination of FOV, sampling rate, instrument response time, and spacecraft speed is such that essentially independent measurements are acquired every 50 km along the subsatellite track. Approximately 211 hours of data and 256 hours of data, respectively, were obtained during the April 9-19 and the September 30 to October 11, 1994, flights [*Connors et al.*, this issue]. The MAPS instrument is robust and carefully calibrated before launch [*Reichle et al.*, 1986, 1990, this issue]. The space-based CO measurements are validated by means of comparisons with scientifically-accepted, independent measurements from nearly 30 stations that range from 71°N to 67° S [*Novelli et al.*, this issue]. The data from both of these ground-based and five airborne platforms are intercalibrated in order to provide an internally consistent, international network of CO measurements that are directly comparable [*Nolf et al.*, 1994; *Reichle*, 1994; *Connors*, 1994].

In the present investigation the global 1 km Pathfinder data [*Eidenshink and Faundeen*, 1994] from the NOAA 11 AVHRR are used to detect fires over India and Burma. The area of study between 10°N-30°N and 85°E-110°E is shown in the enclosed rectangle in Figure 1. The area covers most of Burma, Thailand, Cambodia, and the northeastern portion of India. Also shown in Figure 1 are the four major ecosystems within the area of study. Figure 1a shows the cropland/natural vegetation mosaic (CVNM), Figure 1b shows the evergreen broadleaf forest (EBF), Figure 1c shows the mixed forest areas that are mainly deciduous (MFD), and Figure 1d shows the grassland areas (GL). The CNVM, EBF, MFD, and GL ecosystems occupy 15%, 11%, 10%, and 6% of the study area. About 54% of the area is covered by water and the remaining 1% are other ecosystem classes. The fire counts are discussed for these four ecosystems in section 4. Table 1 shows a summary of the AVHRR data used in this study and pertinent information about the quality of the images. Also shown are the start and end times of the AVHRR images over the area of study and the corresponding SRL-1 overpass times. The second-by-second instantaneous filtered data [*Reichle et al.*, this issue] were used in this study to correlate the fire activities with the MAPS-measured CO concentrations. Note that two images were used both on April 11 and on April 19. The images on April 16 were not used due to problems in calibration. Also shown in Table 1 are the number of scan lines used for each image and the range of latitudes and longitudes.

3. Methodology

3.1. Detection of Fires Using AVHRR Data

The detection of fires using the AVHRR is a well-established procedure. The International Geosphere Biosphere Programme (IGBP) Data and Information System (DIS) brought together a group of scientists to assess the current capabilities for global satellite fire monitoring and produced a comprehensive report on fire monitoring and related topics [*Justice and Dowty*, 1994]. The basic concept for fire detection is the high response in channel 3 of AVHRR compared to that of channel 4. A simple thresholding technique was proposed by *Kaufman et al.* [1990] to detect fires from AVHRR data over South America. The first condition ($T3 \geq 316$ K) ensures that the channel 3 temperatures are closer to the saturation level of the sensor. The second condition ($T3 \geq T4+10$) imposes the condition that channel 3 temperatures be 10°C higher than channel 4 temperatures, thereby insuring that hot surfaces are not counted as fires. The final condition ($T4 \geq 250$ K) requires that channel 4 temperatures be warmer than 250 K to exclude strongly reflective clouds. These thresholds are computationally efficient and adequate for the detection of fires in the South American region. However, these conditions are found to be inadequate for fire detection over other parts of the world due to the different background conditions [*Franca et al.*, 1995; *Belward et al.*, 1994]. Current algorithms [*Prins and Menzel*, 1992, 1994; *Lee and Tag*, 1990; *Justice et al.*, 1996; *Flasse and Ceccato*, 1996] use spectral, spatial, and ancillary information to detect fires.

In the present study, fires are detected using a slight variation of the *Kaufman* [1990] technique. The thresholds used are: (1) $T3 \geq 319$ K, (2) $T3 \geq T4+10$, and $T4 \geq 255$ K. The fire detection scheme is tested by making sure that the detected fire sources have smoke plumes associated with them. Although it is

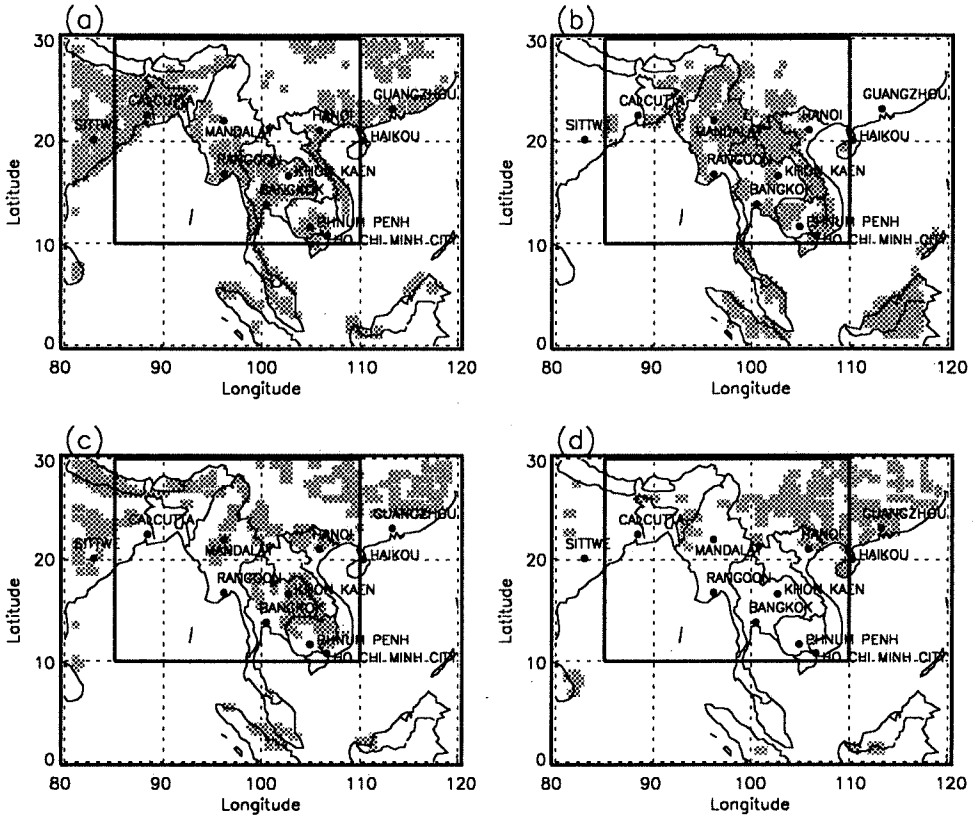

Figure 1. Region of study with four ecosystems: (1) cropland/natural vegetation mosaic (CNVM), (b) evergreen broadleaf forest, (c) mixed forest, and (d) grassland.

not possible to ensure that each fire pixel identified is accompanied by a smoke plume, this method used for fire detection in the current investigation appears to perform well for the area of study. It is noted that although sophisticated contextual algorithms do provide better fire discrimination from the background, the present thresholding technique is both adequate and computationally simple.

3.2. Estimation of Carbon Monoxide Concentrations Using AVHRR Data

During biomass burning, large amounts of the trace gases CO_2, CO, CH_4, and NO_X are released into the atmosphere. The MAPS-measured CO values provide a good source of validation for both the AVHRR-derived estimates and the model-derived values. In the present study, AVHRR data are used to identify the fires and the area covered by these fires on a daily basis. Using emission factors reported by *Kaufman et al.* [1990], CO mixing ratios are calculated for a 25 x 25 AVHRR group of pixels which roughly corresponds to the Instantaneous Field of View (IFOV) of the MAPS radiometer. The carbon monoxide is assumed to be mixed uniformly in this grid box up to an altitude of 8 km, which is the height of the MAPS measurements. It is noted that CO may not be mixed uniformly in the vertical column, so this is an approximation.

The basic assumption used in the estimation of emitted mass of CO (also applicable for methane, CO_2, and other gases) is that there is a direct relationship between the mass of the emitted particulates to the mass of emitted CO. This assumption is supported by field measurements of *Ward and Hardy* [1984] and *Ward* [1986]. Therefore if the mass of the emitted particulates can be estimated from satellite data, then an estimate of the mass of the emitted CO can be obtained. The field measurements used in temperate areas by *Ward and Hardy* [1984] are extrapolated to the tropical regions in Brazil by *Kaufman et al.* [1990]. In the present study, the same relationship is assumed due to lack of other independent measurements.

There are two major phases during biomass burning. The first phase, which is called the "flaming phase," has very high rates of heat release of (1-10 MW/m^2) but has a low rate of release of particulate matter and trace gases. The second phase, called the "smoldering phase," has very low rates of heat release (<0.1 MW/m^2) but has a high rate of release of trace gases and particulate matter. In the present study, computations are only made for smoldering conditions. The following relationship between the mass of the emitted CO and the emitted particulates is assumed following the work of *Ward* [1986].

$$M_{CO} = (17 \pm 5)\, M_P, \tag{1}$$

where M_{CO} is mass of emitted CO, and M_P is mass of emitted particulates.

The next step is to obtain estimates of the mass of the emitted particulates from the AVHRR measurements. For this it is assumed that the observed fires and the resulting emissions can be represented by an "average" fire [*Kaufman et al.*, 1990]. The atmospheric loading (aerosol optical thickness) is calculated from the difference in channel 1 radiances between the smoke-covered area and the clear-sky area nearby. Then, the calculated optical thickness is integrated over the area covered by smoke, and a total mass of smoke is determined. The next step is to calculate a

Table 1. The NOAA11 AVHRR Images Used During April 9-19, 1994, MAPS missions

Day	Block ID	AVHRR		Lat-Range (N)	Lon-Range (E)	Number of lines	No. of fires	Percent Cloud Cover Over Land	MAPS	
		Start time (UT)	End time (UT)						Start time (UT)	End time (UT)
9	2854950	9.27	9.35	8.64-29.99	89.34-121.6	1778	1007	37	10.0	10.08
10	2856364	9.06	9.14	8.64-29.99	92.48-124.75	1773	383	52	19.43 8.22	21.0 9.77
11	2857778 2857979	8.85 10.54	8.94 10.63	8.64-30.0 5.75-30.0	95.62-127.91 70.14-103.0	1778 2087	73 224	56 46	7.9 9.38	7.93 9.45
12	2859192	8.63	8.73	5.74-30.0	98.76-131.64	2089	14	51		
13	2860607	10.12	10.22	5.75-29.98	76.42-109.3	2087	1256	35	18.51 7.28 8.77	18.55 7.28 8.83
14	2862021	9.93	10.01	8.59-29.99	79.55-111.89	1785	3585	33	18.22 6.93 8.43	18.25 6.97 8.5
15	2863435	9.72	9.81	8.59-29.99	82.69-115.04	1785	544	30	17.83 8.1	17.92 8.15
16*										
17	2866263	9.31	9.39	8.62-30.0	88.96-121.35	1781	180	58	17.16 7.42	17.22 7.45
18	2867677	9.10	9.18	8.62-30.0	92.10-124.51	1780	118	41	16.76 5.57 7.05	16.85 5.57 7.07
19	2869191	8.89	8.98	8.6-29.99	95.25-127.67	1781	130	37	11.0	12.5
	2869292	10.58	10.68	5.74-30.0	69.75-102.75	2089	37	30		

* Image not used due to problems in calibrating the image.

conversion factor that links the optical thickness to the mass of aerosol generated per unit area of the surface burned. The mass of emitted particulates is the product of: (1) the number of fires, (2) the area covered by one pixel, (3) the duration of the fires, and a ratio that converts the optical thickness measurements into mass of aerosol-emitted/unit area. The following relation is used to compute M_P:

$$M_P = Q\frac{T_{fire}}{t_{AVHRR}}a_f N \quad (2)$$

where

Q conversion factor used to convert the optical thickness to mass of aerosol emitted per unit area of the surface;
T_{fire} average daily duration of emissions from fires;
t_{AVHRR} duration of emission till the AVHRR image was acquired;
a_f area of the pixel identified as fire;
N number of fires.

The particle radius of the emitted aerosol is taken as an average of the radius derived by using remote sensing techniques (~0.3 μm [*Kaufman et al.*, 1990] and the radius measured in situ (0.15 μm [*Radke et al.*, 1989; *Radke*, 1989]). Assuming a density of 1 g/cm^3, the conversion factor Q is 0.22 g/m^2. Assuming that half of the aerosol mass is liquid water, the conversion factor is 0.11 g/m^2. Assuming that the fires started around 1100-1200 LT and the duration of emission was about 7 hours [*Kaufman et al.*, 1990], the T_{FIRE}/t_{AVHRR} ratio is about 0.5 ± 0.2. It is noted that the aforementioned values are assumptions that require more validation as pertinent data become available.

Kaufman et al. [1990] provide accuracy estimates for the computation of particles and trace gas emissions. The estimated errors are 30% error in the computation of optical thickness [Fraser *et al.*, 1984], 30% error in determining the total aerosol mass from optical thickness [Fraser *et al.*, 1984], 30% error from the computation of dry aerosol mass [Kaufman *et al.*, 1986]; 40% error when converting from dry aerosol mass to emitted trace gases [*Ward*, 1986], and 60% error from the integration over whole area and emission time [*Ferrare et al.*, 1990]. The multiplicative errors therefore lead to an estimate of emissions within a factor of 2. Another source of error is due to the assumption that the entire AVHRR pixel is covered with one fire. Although the AVHRR 3.7 μm channel is sensitive to flaming fires as small as 10 x 10m and smoldering fires of the order of 30 m x 30 m, the AVHRR saturation at around 320 K prevents the separation between flaming and smoldering conditions [*Kaufman et al.*, 1990]. Also, when the pixel saturates, it is not possible to determine the size of the fires. With the new generation of sensors such as the moderate (MODIS) to be launched as part of NASA's Mission to Planet Earth (MTPE) program, these difficulties may be largely overcome. However, it is important to obtain high-quality field experiment data from major ecosystems where biomass burning activities are prevalent.

4. Results

4.1. AVHRR Detection of Fire and Smoke

Plate 1a shows an AVHRR image over the India-Burma border for April 11, 1994. The longitude range is between 87° and 97°E and the latitude range is between 17° and 26°N. The image is approximately 10^6 km^2 in area. This is a typical pseudocolor image, in which channel 1 is in red, the normalized ratio of (1-4)/(1+4) is in green, and the mean textural measure of (1-4)/(1+4) is in blue [*Christopher et al.*, 1996]. The fires are colored in red following the fire detection scheme, as explained in section 3.1. There are 489 fires detected for this image. The white color shows the clouds that are colder than 255 K, and the light yellow color shows the smoke produced from burning. This image was acquired approximately between 1054 and 1063 UT. The MAPS data over this area were acquired between 0938 and 0945 UT. Several interesting features can be noted in Plate 1. Over the Bay of Bengal area the MAPS sensor measured low values (around 60-75 ppbv), shown by the green boxes in Plate 1a. Over the area of active fires around the Indo-Burma border the MAPS sensor measured higher values (between 120 and 135 ppbv) of CO concentrations, as indicated by the yellow boxes in Plate 1a. Several mechanisms have been proposed [*Connors et al.*, 1991; *Pickering et al.*, 1992] for the transport of CO from the boundary layer to the MAPS-measured altitudes, among which deep convection plays an important role. Although there is approximately a 1-hour difference between the MAPS and the AVHRR overpass times, there appears to be a good correlation between the fire activities and the location of MAPS-measured CO concentrations. During April 9-19, 1994, the 850 mbar wind directions from the European Centre for Medium-Range Weather Forecasts (ECMWF) model over Burma were from the southwest with magnitudes around 5-10 m/s, which probably transported the biomass burning aerosols farther inland into China (not shown). At 500 mbar, wind directions were predominantly from the west, with magnitudes around 20-30 m/s, which transported the biomass burning aerosols from the Indo-Burma area into the Pacific Ocean where high values of CO were observed (not shown). The meteorological conditions during this time period are discussed in detail by *Connors et al.* [this issue].

4.2. Carbon Monoxide Measurements From MAPS

In order to examine the fire activities with CO measurements from MAPS, the second-by-second MAPS data over the region of interest were used to create a 1° x 1° gridded product. Plate 1b shows the MAPS-measured CO concentrations. The area of interest is shown in the black square between 85°E -110°E longitude and 10°N-30°N latitude. Also shown in purple circles and triangles are the astronaut-observed smoke and fires. During the April 1994 MAPS emission the astronauts observed both fires and smoke plumes over the region of interest. Note that even at this resolution of 1° x 1°, several regions in the area of interest do not have CO values shown, either due to clouds or due to the lack of overpasses by the space shuttle. The MAPS-measured CO concentration values during the April 1994, mission range from 30 ppbv to about 165 ppbv. Over the Bay of Bengal area, the MAPS-measured CO values are around 30-75 ppbv. Over Bangladesh and northwestern Burma the 10-day average values are around 90-120 ppbv. This increase in CO concentrations is attributed to biomass burning. Another area of high CO concentrations is in Cambodia (107°E, 12°N). However, there were no astronaut-observed fires over this area.

The 10-day composite values of CO concentrations from the MAPS sensor are found to be between 60 and 90 ppbv over the Bay of Bengal area, but over the Indo-Burma border between 90°-95°E longitude and 20°-25°N latitude, CO values are 105-135 ppbv. These high CO values are due to the burning that is prevalent during this season. The astronaut-observed fires also correspond well with the fires detected by the satellite measurements from AVHRR. Also, note the high CO values measured

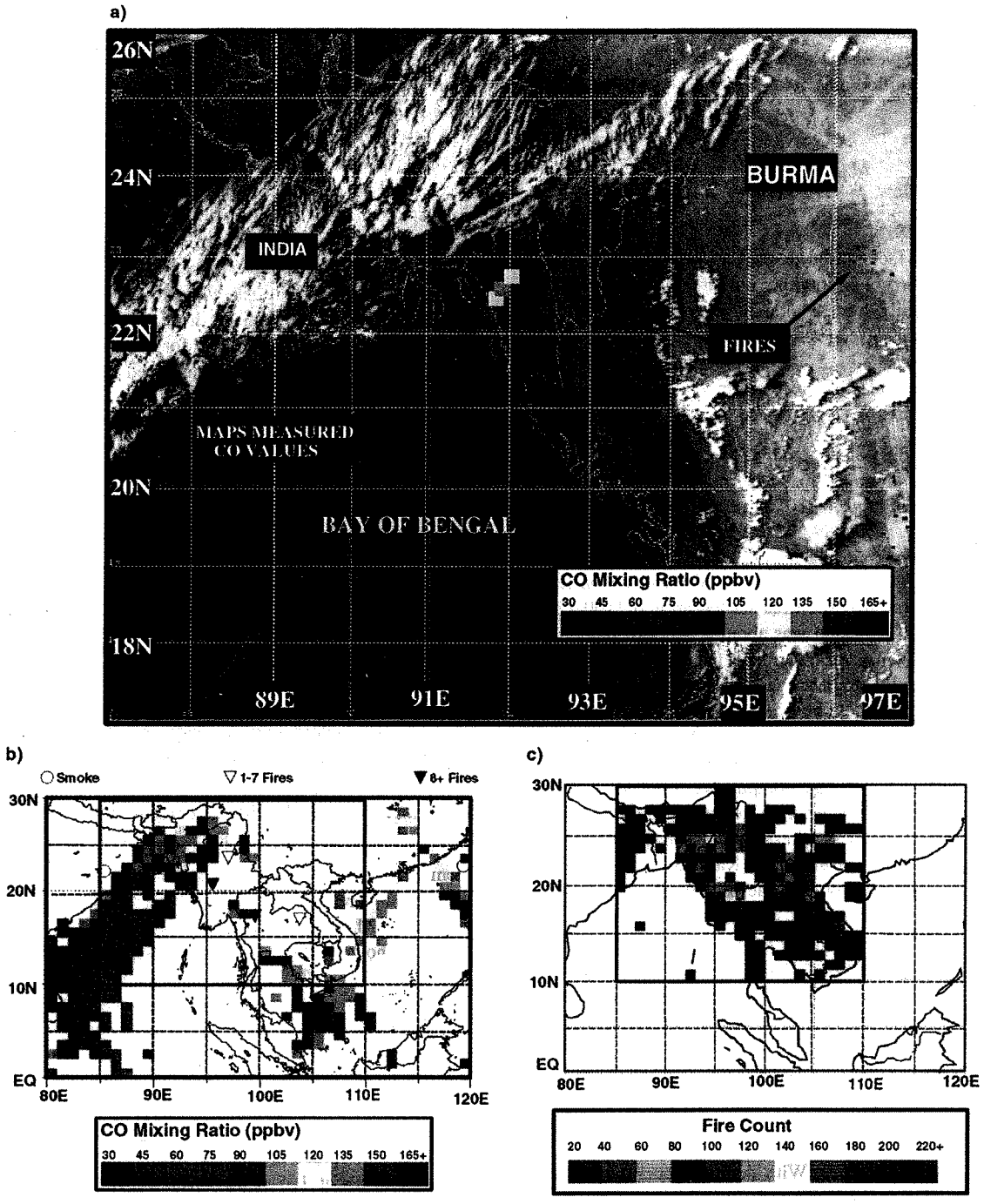

Plate 1. (a) A three-band overlay from advanced very high resolution radiometer (AVHRR) imagery. Channel 1 is in red; ratio of (1-4)/(1+4) is in green, and the mean textural measure of (1-4)/(1+4) is in blue. Fires are denoted in red. Also shown are the MAPS-measured carbon monoxide concentrations. (b) MAPS-measured CO concentrations from the April 9 to 19, 1994, mission on a 1° x 1° degree grid. The astronaut observations of fire and smoke are shown as purple triangles and circles. (c) AVHRR estimations of fires on a 1° x 1° degree grid.

between 100°-110°E longitude and 5°-15°N latitude in Plate 1b. The astronaut-observed fires and smoke correspond well within high values of measured CO values. Comparison of Plates 1b and 1c shows that while there are fire counts made by the AVHRR over many regions, no corresponding MAPS-measured CO values may be shown. This could be due to several reasons. (1) During the times of the MAPS overpass, the field of view could have been obstructed by clouds; (2) no MAPS measurements were made due to the orbital characteristics of the space shuttle; and (3) prevailing winds may have transported the biomass burning particulates away from the source. This effect can be seen in the Pacific Ocean (115°-120°E; 20°-25°N; 110°-115°E; 15°-20°N), where the winds are responsible for the transport of CO from the land to the ocean areas. However, the large CO concentrations are clearly a function of biomass burning activities, as seen in Plates 1b and 1c.

Table 2 shows the number of fires that were detected for each image, along with percent cloud cover information, for each ecosystem. The percent cloud cover information is computed by precluding ocean areas. For example, on April 14, 7.73% of the land area was covered by clouds, and about 770 fires were detected in the remaining 92.27%. More than a thousand fires were detected over the area of interest on April 9, 13, and 14 with peak fire activities on April 14. A total of 7551 fires were detected during the study period out of which the CNVM, EBF, MFD, and GL ecosystems experienced 22%, 43%, 24%, and 9% of the fires, respectively.

Key areas of fires noticed by the astronauts were around south central Bangladesh (90°E, 22°N) and several regions in Burma (95°E, 20°N; 97°E, 24°N) and the northern portion of Thailand (100°E, 18°N; 103°E, 18°N). The number of fires from astronaut observations provides a good qualitative view. Also, note that the astronauts observed smoke plumes in northeastern India (85°E, 22°N) and the western Pacific Ocean around 120°E and 23°N.

Plate 1c shows the results from the AVHRR fire detection scheme. The number of fires ranged from 20 to over 200. Peak fire activities were observed in several areas. Fire counts greater than 200 were observed in the Bangladesh-Burma border around 92°E and 22°N. This high number of fires over this area corresponds well to the observations made by astronauts, as shown by the triangles in purple in Plate 1c. This area also showed high CO concentrations (120-135 ppbv), as measured by MAPS. Clearly, there is a direct relationship between the number of fires observed by AVHRR and the MAPS-measured CO values. However, the mechanism for transporting the CO from the boundary layer to the MAPS measurement altitude of 8 km must be carefully explored. Both vertical transport by convective clouds and horizontal transport by the prevailing winds are important in determining the spatial distribution of CO. The other area where high fire counts were observed by the AVHRR is in northeastern Burma (94°E, 25°N). The observed number of fires was around 140. The MAPS-measured CO concentrations were around 105-120 ppbv. In these two areas, there appears to be a direct vertical transport of CO from the boundary layer to the free troposphere. Fire counts of about 140-160 were also observed in southern Burma around 97°E and 18°N, and the observed CO concentrations were around 105-120 ppbv. High values of CO concentrations around 135-150 ppbv were also observed around eastern Thailand by MAPS. Neither AVHRR nor astronaut observations showed increased fire activities in this area. It is speculated that other transport mechanisms may have been responsible for these high values. In summary, the number of fires detected by the AVHRR qualitatively correlate well with MAPS-measured CO concentrations.

As a first attempt toward comparing the MAPS-measured CO concentrations with the AVHRR-derived estimations, the fire counts for the 1° x 1° grids were used as input to a simple model (see section 3.2). In this model, a direct relationship between the mass of emitted CO and the mass of emitted particulates is assumed. This assumption, coupled with a rough estimate of the duration of fires, is used to convert the mass of emitted CO to a free tropospheric carbon monoxide concentration at the MAPS

Table 2. Number of Fires and Percent Cloud Cover Over Land for Each Ecosystem

	Number of Fires				Percent Cloud Cover Over Land			
Day	CNVM	EBF	MFD	G	CNVM	EBF	MFD	G
9	83	684	187	43	7.53	3.09	6.7	7.11
10	39	241	58	6	7.94	2.83	7.63	8.31
11	120	112	15	33	7.35 8.74	2.72 2.56	7.88 7.01	8.26 6.20
12	0	0	0	13	8.24	2.52	7.01	6.43
13	425	499	121	162	7.79	3.13	6.62	5.58
14	770	1232	1290	293	7.73	3.63	6.35	5.24
15	99	294	88	55	7.57	3.87	6.17	5.04
17	27	111	23	16	7.77	4.97	6.59	5.69
18	45	26	3	38	7.65	5.08	6.61	5.56
19	69	19	16	57	7.41 7.26	4.99 4.88	6.43 6.08	5.39 5.01

CNVM, cropland/natural vegetation mosaic; EBF, evergreen broadleaf forest; MFD, mixed forest deciduous; G, grassland.

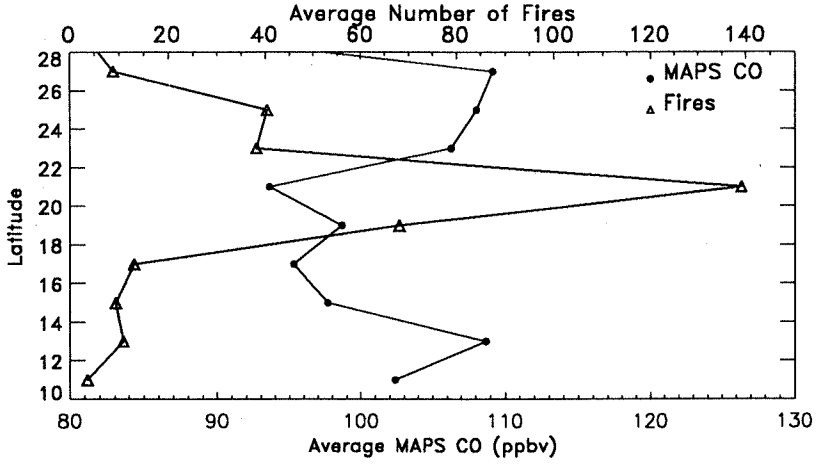

Figure 2. Latitudinal distribution of MAPS-measured CO and AVHRR-detected fire pixels.

measurement altitude of 8 km. The estimated CO mixing ratios from the AVHRR, in parts per billion by volume, in the free troposphere for a 1° x 1° grid, range between 0.1 and 30 ppbv. The AVHRR-derived CO-mixing ratio values are smaller than the MAPS-measured values by a factor of 4 to 5. For example, the AVHRR estimates provide a value of about 30 ppbv at the Bangladesh-India border (22°N, 92°E), while the MAPS-measured values are around 120 ppbv. While the differences in CO concentrations between AVHRR and MAPS are about 4 over Bangladesh, other areas could differ by a factor of 8 to 12. One of the key limitations of this preliminary study is the lack of transport mechanisms to allow for the CO to reach regions other than only over direct fires. This is evident in Plate 1c over the latitude region between 20°-25°N and 90°-95°E. For example, while for the 1° x 1° grid over Bangladesh (22°N, 92°E) the estimated CO mixing ratio is 30 ppbv, in the area north, next to this grid box, no fires were encountered, therefore no CO values were calculated. On the other hand, the MAPS-measured values show a general increase of CO concentrations in this latitude-longitude region when compared with the oceanic areas.

Figure 2 shows the latitudinal distribution of MAPS-measured CO concentrations for the area of study. The CO values are averaged between 85°E and 110°E and include averages over both land and ocean areas. Also shown in this figure are the average number of fires, which are only applicable for land areas. The CO values have two maxima, one between 24°N and 26°N and the other between 12° and 14°N. The corresponding fire counts are around 30-40 for the first peak and around 10-15 for the second peak. The maximum fire counts of around 140 are found in the region between 20° and 22°N, whereas the corresponding MAPS-measured values are around 95 ppbv. This figure indicates that even though high CO concentrations are found around the fire activities, transport mechanisms are important. This is also well demonstrated in Figure 3, which indicates the importance of transport mechanisms that are responsible for enhanced CO concentrations downwind of the biomass burning areas. Figure 3 shows the longitudinal distribution of CO and fires over the area of study. Peak CO values of around 140 ppbv are found in eastern China and the Pacific Ocean, which are downwind of the biomass burning sources in eastern India and Burma. Peak fire counts of around 120 are found between 94° and 96°E due to biomass burning in Burma.

5. Summary and Conclusions

Carbon monoxide is an important reactive trace gas in the atmosphere and plays a crucial role in atmospheric chemistry and climate. Therefore it is vital that we obtain information about the sources and sinks and CO and also to monitor the vertical and spatial distribution. To date, estimations of CO concentrations are solely from ground-based measurements or from atmospheric chemistry modeling. The only direct measurements of CO concentrations from space are from the MAPS instrument. Three MAPS missions have been conducted thus far to study the tropospheric CO concentrations at an altitude of 8 km. The first mis-

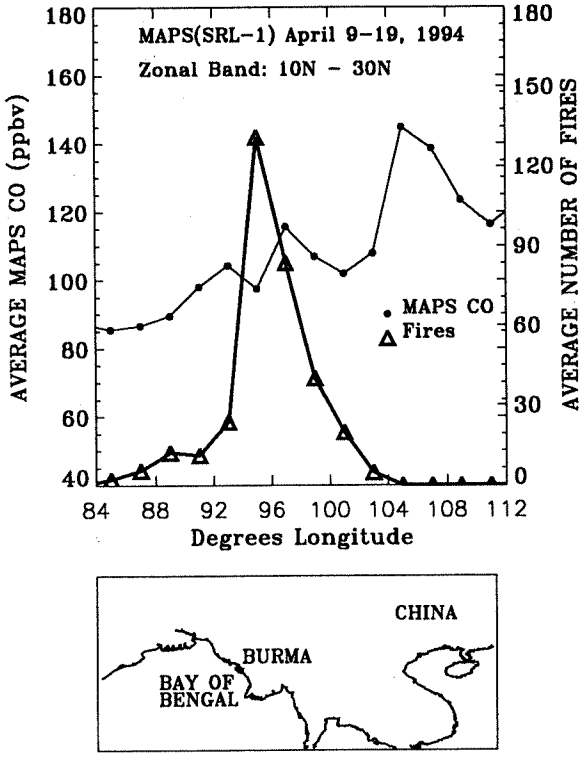

Figure 3. Longitudinal distribution of MAPS-measured CO and AVHRR-detected fires.

sion, conducted in October 1984 [*Reichle et al.*, 1990], measured CO for approximately 5 days. More recently, the MAPS sensor measured both CO and N_2O in April and October 1994 for about 20 days. While most of the emitted CO is from biomass burning, much information is needed by the atmospheric chemistry community to model the effects of CO. Of fundamental importance are the number of fires, their location, and duration. As a first step toward achieving that goal, this study compares the fire activities detected by the AVHRR with the MAPS-measured values over an area between 85°-110°E and 10°-30°N. Ten days of the global 1 km Pathfinder data has been used for this purpose. Using published relationships between particulate and emission concentrations, the AVHRR-detected number of fires are used to obtain estimates of CO in the free troposphere. Although several assumptions are involved in the AVHRR-derived CO concentrations, the method has good potential for estimating CO values on a routine basis.

The results are summarized as follows.

1. The AVHRR data show a number of fires over the Indo-Burma border during the April 1994 missions. These fire activities show an increase in MAPS-measured CO values when compared with the values over the Bay of Bengal area. This qualitative correlation between the fire activities and the high CO concentrations demonstrates a direct relationship.

2. The astronaut-observed fires roughly correspond well to the AVHRR-detected fires. The AVHRR-detected fires provide more quantitative information about the spatial distribution of fires. Note that these fire counts were made from instantaneous satellite imagery, fires of short duration that may have been missed. Also, it is difficult to resolve subpixel fires from satellite imagery that could have an impact on the estimation of the number of fires. Nevertheless, satellite imagery provides the only means for detecting fires on a global basis.

3. For the entire April 1994 MAPS mission, fire counts were made on a 1° x 1° grid. The maximum number of fires at this resolution is around 200 and compares well with enhanced CO values as measured by MAPS. In general, the spatial distribution of fires correspond well to the CO values as measured by MAPS.

4. As a preliminary investigation, the AVHRR-detected number of fires were used to obtain CO concentrations. Several assumptions were used in this estimation regarding the duration of fires, the phase of burning (smoldering or flaming), etc. The spatial distribution of CO estimated from the AVHRR compares well with that of the MAPS measurements. However, the AVHRR-derived values are less than those of the MAPS values by a factor of 4 to 5. The differences are attributed to the various assumptions involved.

In conclusion, the AVHRR measurements play a key role in monitoring the spatial extent of fires. One limitation of the AVHRR satellite is the poor temporal resolution. This could be compensated by using measurements from the new generation of GOES instruments. However, the GOES8 and GOES9 fire and emission products can only be accomplished at 4 km. In this regard, the trade-offs between the temporal and spatial resolution need to be carefully examined. Using available information on CO emissions and particulate matter, this study has examined the utility of the AVHRR to derive CO concentrations.

Acknowledgments. This research was funded by NASA grants NAGW-3966, managed by Robert J. Curran and NAGW-5195 by Dr. Ghassen Asrar. The Pathfinder data used by the authors in this study include data produced through funding from the Earth Observing System Pathfinder Program of NASA's Mission to Planet Earth in cooperation with National Oceanic and Atmospheric Administration. The data were provided by the Earth Observing System Data and Information System, Distributed Active Archive Center at EROS Data Center, which archives, manages, and distributes the data set. Special thanks to Dan Baldwin for the navigation software and Scott Nolf for the MAPS figures. Appreciation is extended to Connie Crandall for organizing this manuscript.

References

Belward, A. S., P. J. Kennedy, and J-M Gregoire, The limitations and potential of AVHRR GAC for continental scale studies, *Int. J. Remote Sens., 15*(11), 2215-2234, 1994.

Cahoon, D. R., Jr., B. J. Stocks, J. S. Levine, W. R. Cofer III, and K. P. O'-Neill, Seasonal distribution of African savannah fires, *Nature, 359*, 812-815, 1992.

Christopher, S. A., D. V. Kliche, J. Chou, and R. M. Welch, First estimates of the radiative forcing of aerosols from biomass burning using satellite data, *J Geophys. Res., 101*, 21,265-21,273, 1996.

Connors, V. S., The grand global carbon monoxide (CO) experiment of 1994, *Eos Trans. AGU, 75*(44), Fall Meet. Suppl., 128, 1994.

Connors, V.S., D. Cahoon, H. Reichle, E. Brunke, M. Garstang, W. Seiler, and H. Scheel, Savanna burning and convective mixing in Southern Africa: Implications for CO emissions and transport, *Global Biomass Burning*, edited by J. Levine, pp. 147-154, MIT Press, Cambridge, Mass., 1991.

Crutzen, P. J., and M. O. Andreae, Biomass burning in the tropics: Impact on atmospheric chemistry and biogeochemical cycles, *Science, 250*, 1669-1678, 1990.

Crutzen, P. J., L. E. Heidt, J. P. Krasnec, W. H. Pollock, and W. Seiler,: Biomass burning as a source of atmospheric gases CO, H_2, N_2O, NO, CH_3Cl, and COS, *Nature, 282*, 253-256, 1979.

Eidenshink, J. C., and J. L. Faundeen, The 1km AVHRR global land data set: First stages in implementation, *Int. J. Remote Sens., 15*(17), 3443-3462, 1994.

Ferrare, R.A., R.S. Fraser, and Y.J. Kaufman, Satellite measurements of a large-scale air pollution: Measurements of forest fire smoke, *J. Geophys. Res., 95*, 9911-9925, 1990.

Flasse, S.P., and P. Ceccato, A contextual algorithm for AVHRR fire detection, *Int. J. Remote Sens., 17*, 419-424, 1996.

Franca, J.R., J.-M. Brustet, and J. Fontan, Multispectral remote sensing of biomass burning in West Africa, *J. Atmos. Chem., 22*, 81-110, 1995.

Fraser, R.S., Y.J. Kaufman, and R.L. Mahoney, Satellite measurements of aerosol mass and transport, *Atmos. Environ., 18*, 2577-2584, 1984.

Justice, C.O., and P. Dowty (Eds.), *IGBP-DIS Satellite Fire Detection Algorithm Workshop Technical Report*, 88 pp., 1994.

Justice, C.O., J.D. Kendall, P.R. Dowty, and R.J. Scholes, Satellite remote sensing of fires during the SAFARI campaign using the NOAA advanced very high resolution radiometer data, *J. Geophys. Res., 101*, 23,851-23,863, 1996.

Kaufman, Y. J., and T. Nakajima, Effect of Amazon smoke on cloud microphysics and albedo: Analysis from satellite imagery, *J. Appl. Meteorol., 32*, 729-744, 1993.

Kaufman, Y.J., T.W. Brakke, and E. Eloranta, Field experiment to measure the radiative characteristics of a hazy atmosphere, *J. Atmos. Sci., 43*, 1135-1151, 1986.

Kaufman, Y. J., C. J. Tucker, and I. Fung, Remote sensing of biomass burning in the tropics, *J. Geophys. Res., 95*, 9927-9939, 1990.

Kennedy, P., Biomass burning studies: The use of remote sensing, *Ecol. Bull., 42*,133-145, 1992.

Lee, T. F., and P. M. Tag, Improved detection of hotspots using the AVHRR 3.7 μm channel, *Bull. Amer. Meteorol. Soc., 71*, 1722-1730, 1990.

Logan, J. A., M. J. Prather, S. C. Wofsy, and M. B. McElroy, Tropospheric chemistry: A global perspective, *J. Geophys. Res., 86*, 7210-7254, 1981.

Nolf, S.R., V.S. Connors, H.G. Reichle Jr., and P.C. Novelli, Measurements of trace gas constituents from ground-based, airborne, and spaceborne platforms II posters, *Eos Trans. AGU*, Fall Meet. Suppl., *75*(4), 147, 1994.

Novelli, P.C., *et al.*, An internally consistent set of globally distributed atmospheric carbon monoxide mixing ratios developed using results from an intercomparison of measurements. *J. Geophys. Res.*, this issue.

Penner, J. E., R. E. Dickinson, and C. A. O'Neill, Effects of aerosol from biomass burning on the global radiation budget, *Science, 256*, 1432-1433, 1992.

Pickering, K.E., J.R. Scala, A.M. Thompson, W.K. Tao, and J. Simpson, A regional estimate of convective transport of CO from biomass burning, *Geophys. Res. Lett.*, *19*(3), 289-292, 1992.

Prins, E.M. and W.P. Menzel, 1992: Geostationary satellite detection of biomass burning in South America. *Int. J. Rem. Sens.*, *13*(15), 2783-2799.

Prins, E.M., and W.P. Menzel,1994: Trends in South American biomass burning detected with the GOES visible infrared spin scan radiometer atmospheric sounder from 1983-1991. *J. Geophys. Res.*, *99*(D8), 16 719-16 735.

Radke, L.F., Airborne observations of cloud microphysics modified by anthropogenic forcing, in *Procedings of the Symposium on Atmospheric Chemistry and Global Climate*, Am. Meteorol. Soc., Boston, Mass., 1989.

Radke, L.F., J.A. Coakley Jr., and M.D. King, Direct remote sensing observations of ships on clouds, *Science*, *243*, 57-63, 1989.

Reichle, H. G., Jr., Spaceborne tropospheric carbon monoxide, past, and future, *Eos Trans. AGU*, Fall Meet. Suppl., *75*(44), *128*, 1994.

Reichle, H. G., Jr., V. S. Connors, J. A. Holland, W. D. Hypes, H. A. Wallio, J. C. Casas, B. B. Gormsen, M. S. Saylor, and W. D. Hesketh, Middle and upper tropospheric carbon monoxide mixing ratios as measured by a satellite-borne remote sensor during November 1981, *J. Geophys. Res.*, *91*, 10,865-10,887, 1986.

Reichle, H. G., Jr., V. S. Connors, J. A. Holland, R. T. Sherrill, H. A. Wallio, J. C. Casas, E. P. Condon, B. B. Gormsen, and W. Seiler, The distribution of middle tropospheric carbon monoxide during early October 1984, *J. Geophys. Res.*, *95*, 9845-9856, 1990.

Reichle, H.G., Jr., B.B. Gormsen, and V.S. Connors, Space shuttle based global CO measurements during April and October 1994, MAPS instrument, data reduction, and data validation, this issue.

Seiler, W., and P. J. Crutzen, Estimates of gross and net fluxes of carbon between the biosphere and the atmosphere from biomass burning, *Clim. Change*, *2*, 207-247, 1980.

Setzer, A. W., and M. C. Pereira, Amazonia biomass burnings in 1987 and an estimate of their tropospheric emissions, *Ambio*, *20*(1), 19-22, 1991.

Ward, D. E., Field scale measurements of emissions from open fires, technical paper, Def. Nucl. Agency Global Eff. Rev., Def. Nucl. Agency, Washington, D.C., 1986.

Ward, D.E., and C.C. Hardy, Advances in the characterization and control of emissions from prescribed fires, in *Proceedings of the 77th Annual Meeting, Air Poll. Control. Ass.*, San Francisco, Calif., 1984.

S. A. Christopher (corresponding author), J. Chou, and R.M. Welch, Department of Atmospheric Sciences, University of Alabama in Huntsville, 977 Explorer Blvd., Huntsville, Alabama 35899. e-mail: sundar@atmos.uah.edu.

D.V. Kliche, Institute of Atmospheric Sciences, South Dakota School of Mines and Technology, 501 East St. Joseph Street, Rapid City, SD.

V. S. Connors, NASA Langley Research Center, Atmospheric Sciences/MS 483, 21 Langley Blvd., Hampton, VA.

(Received October 4, 1996; revised May 28, 1997;
accepted June 9, 1997.)